Interpretation of phase reversals in seismic reflections from attenuating targets

Xiaoyang Wu[1], Mark Chapman[2], Erika Angerer[3]

1. Edinburgh Anisotropy Project, British Geological Survey, Murchison House, West Mains Road, Edinburgh EH9 3LA, UK.

2. School of Geosciences, University of Edinburgh, The King's Buildings, West Mains Road, Edinburgh, EH9 3JW, UK.

3. OMV Exploration & Production, Gerasdorfer Straße 151, 1210 Vienna, Austria.

Abstract

Phase reversals are commonly observed during exploration seismic amplitude-versus-offset analysis, and usually modelled with the Zoeppritz equations. In practice, when multiple fluids are present we often deal with reflections from interfaces having a contrast in both elastic and anelastic properties. In this paper, we present a new phenomenological model for phase reversals in cases in which velocity dispersion and attenuation are present. We demonstrate strong qualitative differences in behaviour between the elastic and anelastic cases, influencing both the amplitude and phase of the reflection coefficient. Analysis of seismic data showing a phase reversal from a gas reservoir in the Vienna basin shows a striking agreement with the modelling. We conclude that the influence of fluid-induced dispersion on reflection data is a significant and measurable phenomenon in cases of practical interest, that recognition of the phenomena may be used as a novel fluid indicator and that frequency-dependent rock physics analysis may be an important tool for both industrial geophysics and seismic monitoring of CO_2 storage.

Key words

Phase reversal; Frequency domain; Rock physics; Seismic exploration

Introduction

Phase reversals are an important feature which can often be observed during seismic Amplitude Versus Offset (AVO) analysis. Rutherford and Williams (1989) introduced the now standard classification system which suggests that the reversals are most prevalent for reflections where there is a weak normal incidence reflection coefficient, typically referred to as a class II AVO. Class II AVO reflections were further subdivided by Ross and Kinman (1995) into those with phase reversals (also known as class IIp) and those without phase reversals. Castagna and Swan (1997) introduced the class IV AVO concept, these reflections have a negative normal incident reflection coefficient but a decrease in amplitude with offset, and such reflections can show phase reversals. Numerous examples of phase reversals have been published in the literature (Widess, 1973; Ross and Kinman, 1995; Castagna et al., 1998; Roden et al, 2005; van der Baan et al., 2010; Edgar and Selvage, 2011).

Much recent research in the literature has focussed on linking fluid saturation to seismic velocity dispersion and attenuation (Pride et al., 2004; Batzle et al. 2006; Müller and Rothert, 2008, Müller et al., 2010; Quintal and Tisato, 2013; Tisato and Quintal, 2013). The impact of such effects on seismic reflection data has also been theoretically studied (Chapman et al., 2006; Innanen, 2011). Attention has focussed primarily on how the amplitude of the reflection coefficient varies with frequency, and an extended version of the Rutherford and Williams (1989) classification system has been developed for cases where the reflecting layer exhibits strong dispersion. The theory predicts that fluid-induced dispersion should boost the low frequencies of class III AVO reflections and the high frequencies of class I AVO reflections, provided that no phase reversals are present. The concepts have theoretical potential, but the practical applicability is still unclear. An additional cause of the frequency-dependence of reflection coefficients is the tuning effect from thin layers, which is studied by Liu and Schmitt (2003), Korneev et al.(2004) and Quintal et al.(2011).

In this paper, we focus on the effects of attenuation and velocity dispersion in models which exhibit phase reversals. We consider a strongly attenuating fluid-saturated medium overlaid by a medium with elastic properties. The behaviour in these cases turns out to be markedly different from the classical model of a phase reversal, and includes important effects on both the amplitude and phase of the reflections. We begin by briefly outlining the mathematical theory, before studying a number of numerical models. Then, we show a field data example which exhibits the features predicted by the modelling. Finally, we discuss the potential application of such effect and frequency-dependent rock physics models in quantitative estimation of gas saturation and monitoring of CO2 storage in brine-filled reservoir from seismic data.

Theory

The use of Zoeppritz equation (1909) for exact calculation of reflectivity between two elastic half spaces has been well known for over one hundred years. Numerous simplifications have been proposed and applied to AVO analysis (Aki and Richards, 1980; Shuey, 1985; Smith and Gidlow, 1987). When reflection comes from fluid saturated medium, reflectivity becomes frequency-dependent due to velocity dispersion. The frequency-dependent reflectivity can be calculated through combination of rock physics models, which consider frequency-dependent elastic stiffness, with the Zoeppritz equation. We use Chapman et al. (2002) squirt model that considers the fluid exchange between pores and cracks, as well as between cracks of different orientations due to wave propagation, which give rise to the frequency-dependent effective elastic moduli:

$$c_{ijkl}(\omega) = c^0_{ijkl} - \varphi_p c^1_{ijkl}(\omega) - \varepsilon_c c^2_{ijkl}(\omega)\ , \qquad (1)$$

where c^0 is the isotropic elastic tensor, c^1, c^2, are the contributions from pores and microcracks. φ_p is porosity, ε_c is crack density, ω is angle frequency. When the rock is partially saturated with two immiscible fluids, the bulk modulus and density of the effective

fluid are estimated by Wood's Formula (Wood, 1955), and the viscosity is averaged arithmetically in terms of volume percentage of each fluid.

For the calculation of reflectivity, we use an extended version of the formulation presented by Schoenberg and Protazio (1992). Since the upper layer is elastic, the wavefield may be written in exactly the same form as used by Schoenberg and Protazio (1992),

$$\begin{bmatrix} v_1 \\ v_2 \end{bmatrix} = i_p \begin{bmatrix} \alpha s_1 \\ \alpha s_{3_p} \end{bmatrix} \exp \mathrm{i}\omega s_{3_p} x_3 + r_p \begin{bmatrix} \alpha s_1 \\ -\alpha s_{3_p} \end{bmatrix} \exp -\mathrm{i}\omega s_{3_p} x_3$$

$$+ i_s \begin{bmatrix} \beta s_{3_p} \\ \beta s_1 \end{bmatrix} \exp \mathrm{i}\omega s_{3_s} x_3 + r_s \begin{bmatrix} \beta s_{3_s} \\ \beta s_1 \end{bmatrix} \exp -\mathrm{i}\omega s_{3_s} x_3, \quad (2)$$

Where $s_{3_p} = \sqrt{\alpha^2 - s_1^2}$, $s_{3_s} = \sqrt{\beta^2 - s_1^2}$, α and β are the P and S wave velocities, s_1 is the horizontal slowness. We assume a single incident P-wave giving rise two reflected P and S waves, what follows we will take the incident amplitude i_p to be equal to 1.

To construct the wavefield in the lower layer, we must take account of the frequency-dependent properties. Following the equation (2), stress σ and strain ε are related through the equation,

$$\sigma_{ij} = c_{ijkl}(\omega)\varepsilon_{kl}. \quad (3)$$

The wavefield in the lower layer consists of transmitted P and SV waves, and will have displacements of the form,

$$u = t_p \begin{bmatrix} e_{p_1} \\ e_{p_2} \end{bmatrix} \exp \mathrm{i}\omega \left(s_1 \mathrm{x} + s_{3_p} \mathrm{z} - t \right) + t_s \begin{bmatrix} e_{s_1} \\ e_{s_1} \end{bmatrix} \exp \mathrm{i}\omega \left(s_1 \mathrm{x} + s_{3_s} \mathrm{z} - t \right) \quad (4)$$

The horizontal slowness s_1 must be the same as in the upper layer, and we obtain the vertical slownesses and polarizations through the Christoffel equation. We define the Christoffel matrix as,

$$\Gamma_{jl} = c_{ijkl} s_i s_k, \quad (5)$$

allowing the vertical slownesses to be obtained from the equation,

$$\left| \rho \delta_{jl} - \Gamma_{jl} \right| = 0. \quad (6)$$

The polarizations are given as the corresponding eigenvectors of the Christoffel matrix Γ_{jl}.

Having calculated the wavefield parameters, the reflection coefficients can be calculated from impedance matrices as was done by Schoenberg and Protazio(1992). Specifically, for each frequency ω, we calculate a reflection matrix of the form,

$$R = (Y'^{-1}Y + X'^{-1}X)^{-1}(Y'^{-1}Y - X'^{-1}X), \quad (7)$$

where X and Y, X' and Y' have the same definitions as in equation (14) of Schoenberg and Protazio(1992).

Numerical modelling

We illustrate the theory by considering a number of numerical models which display the phase reversal behaviour. The numerical modelling is performed using ANISEIS software, in which the methods are based on the reflectivity method using materials with frequency-dependent properties. The source used in the modelling is a Ricker wavelet with 40Hz dominant frequency. Attention is focussed on the PP reflection coefficient of two models, one of which is a typical class IIp AVO example, with the other being a class IV AVO example. In both models, an anelastic reference material with certain porosity and water saturation is designed for the lower layer. Then the dispersion and attenuation properties for other scenarios of porosity and water saturation combination can be calculated by incorporating Wood's Formula. The models parameters are listed in Table 1.

Table 1 The parameters for the two-layer model with shale overlying fluid saturated sandstone.

	Layers	Vp (km/s)	Vs (km/s)	Density (g/cm^3)	Thickness (km)	Porosity	Sw
Model 1 (Class IIp AVO)	Upper	2.775	1.408	2.06	1		
	Lower (reference)	2.790	1.463	2.08	Half space	0.30	1.00
Model 2 (Class IV AVO)	Upper	3.200	1.570	2.50	1		
	Lower (reference)	3.100	1.450	2.29	Half space	0.16	0.90

Kw = 2.0GPa; Kg = 0.2GPa;

We treat both the frequency-independent (elastic) and frequency-dependent (anelastic) cases separately to focus attention on the qualitative differences. In each case we calculate both the reflection coefficients and full waveform synthetics. Instantaneous phase of waveform data is estimated following the method of Taner et al.(1979), in which the instantaneous phase of seismic signal $s(t)$ is estimated by arctan function of the ratio of real part and imaginary part of its complex signal.

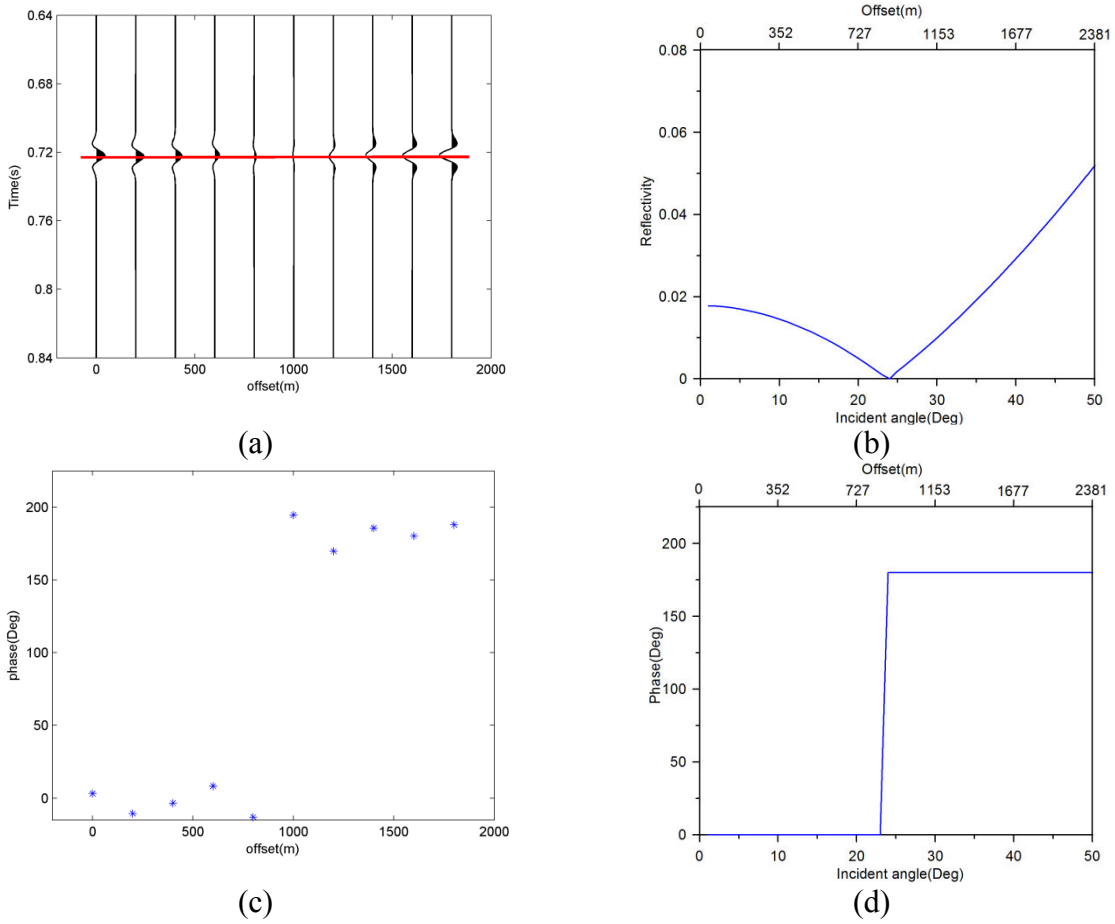

Figure 1. The synthetic waveform, theoretical reflectivity and phase variation at the interface for model 1, when dispersion and attenuation are not considered for the lower medium. (a)The synthetic waveform. A phase reversal of amplitude from positive to negative can be clearly seen. (b) Theoretical reflectivity, reflectivity reduces to zero and then bounce back; (c)The phase variation of the synthetic waveform (a) at the time position as indicated by the red line. Phase changes suddenly from 0^o to 180^o; (d) the theoretical phase variation.

Figure 1 shows the first model for the case in which there is no attenuation or velocity dispersion. This is a typical class IIp AVO example. In the synthetic waveforms of elastic model (a), where dispersion and attenuation are not introduced into the lower half-space, the events have been aligned by time-shift to eliminate the complications of NMO stretch (Dunkin and Levin, 1973). The maximum amplitudes of the event for non-zero-offset traces is shifted to the same level as that of zero-offset trace. These same shift distances are applied in each subsequent dispersive model. In the elastic case, the reflection coefficient is frequency-independent and has a phase jump from 0^o to 180^o discontinuously at the reversal. The amplitude of the reflection coefficient is 0 at the reversal offset, and this is apparent on the waveform data. Estimating the phase from the waveform data using the Hilbert transform, we see a discontinuous change (c), mirroring the behaviour of the theoretical reflection coefficient (b) and phase change (d).

The introduction of dispersion and attenuation in the lower half-space changes the predicted behaviour significantly. Figure 2 shows the results of repeating the analysis with attenuation and dispersion. The P-wave and S-wave velocity dispersion and attenuation as a function of frequency are displayed in (a) and (b), respectively. Comparing the waveform data (c) to the previous example, the most obvious difference lies in the amplitude. In comparison to the elastic modelling, the amplitudes do not approach zero at the point of the phase reversal. Examining the phase in (d), we see a much more continuous phase shift from 50^o to 150^o.

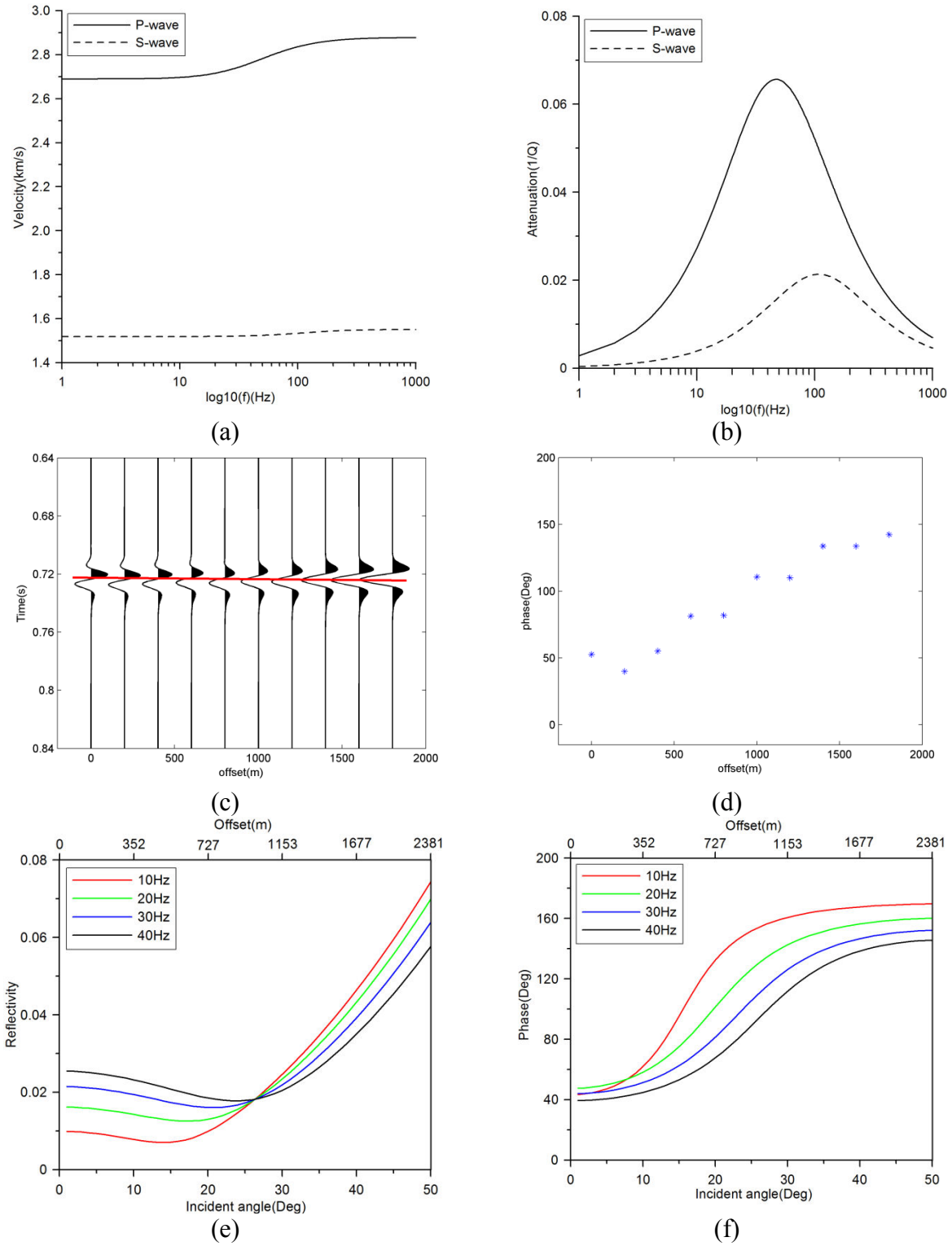

Figure 2 The dispersion and attenuation, synthetic waveform, theoretical reflectivity and phase variation at the interface for the lower medium of model 1. (a)The P-wave and S-wave velocity dispersion for the lower medium; (b)The P-wave and S-wave attenuation (1/Q) versus frequency for the lower medium; (c)The synthetic waveform. (d)The phase variation of

the synthetic waveform (c) at the time position as indicated by the red line, phase changes gradually from 50^o to 150^o. (e) Theoretical reflectivity. The reflectivity at different frequencies crosses at a certain incident angle without hitting zero. Before crossing, reflectivity increases with increasing frequency. After crossing, reflectivity decreases with increasing frequency; (f) The theoretical phase of reflection coefficient versus angle of incidence.

This behaviour can be understood by examining the behaviour of the reflection coefficients in Figure 2(e) and (f). The velocity dispersion and attenuation give rise to a complex reflection coefficient whose phase and amplitudes vary with frequency. As can be seen from Figure 2(f), the phase of the reflection coefficient varies smoothly due to velocity dispersion and attenuation, not discontinuously as in the elastic case. Figure 2(e) shows that the amplitudes of the reflection coefficients are always non-zero. For near vertical incidence, the high frequencies are more reflective, but the opposite is the case after the nominal phase reversal.

Figure 3 repeats the analysis for a case (model 2 as shown in Table 1) with a high-to-low impedance contrast. This is similar to a class IV AVO type behaviour, with a negative intercept and positive gradient. Qualitatively, the predicted behaviour is similar to that observed in Figure 2. The major difference is seen in the amplitudes of the reflection coefficients. In this case, it is the low-frequencies which have higher reflectivity for small angles of incidence, and the high frequencies which are more reflective for higher angles of incidence.

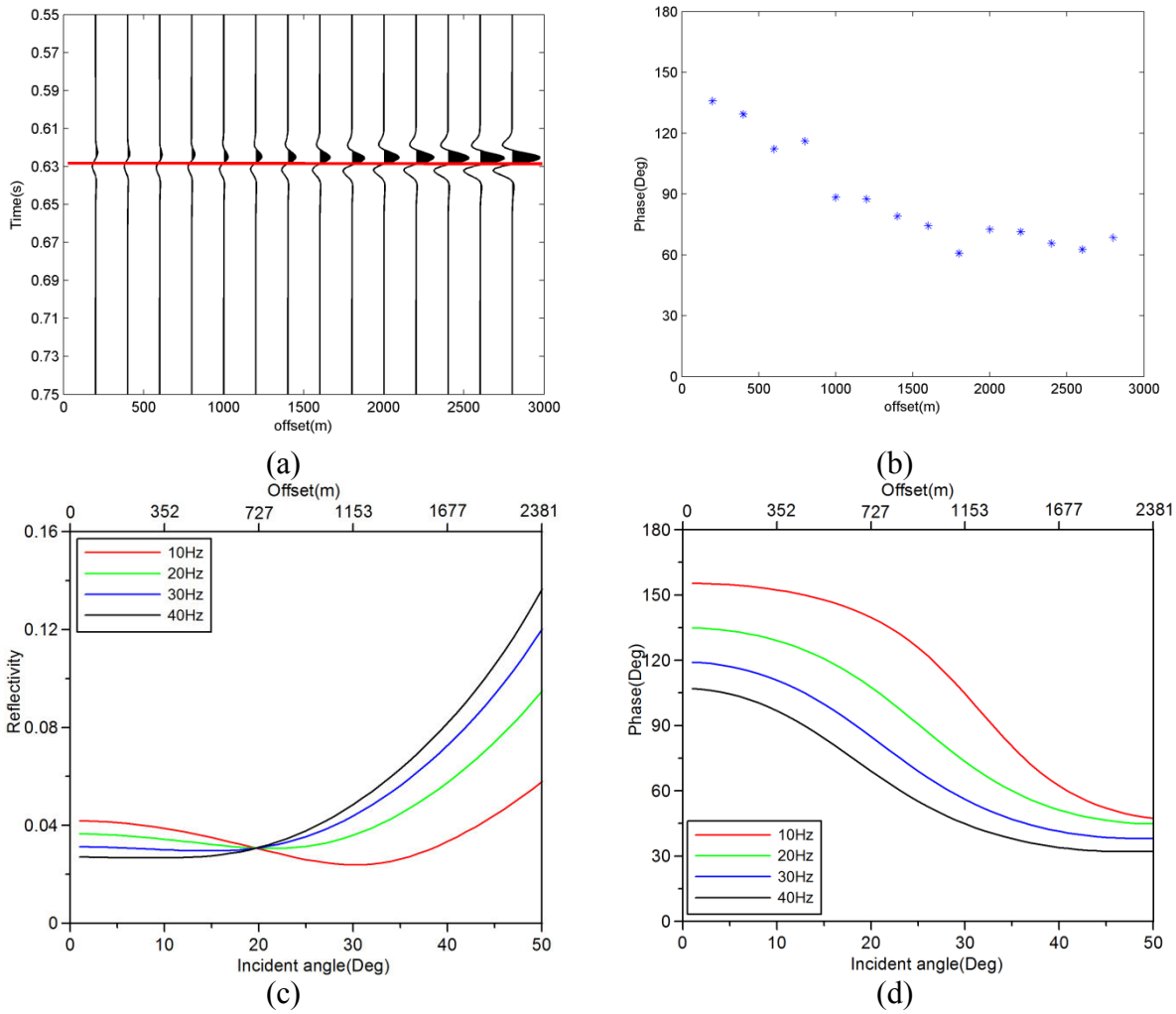

Figure 3 The synthetic waveform, theoretical reflectivity and phase variation at the interface for model 2 when dispersion and attenuation are considered for the lower medium. (a)The synthetic waveform. (b)The phase variation of the synthetic waveform (a) at the time position as indicated by the red line, phase changes gradually from around 140^o to 60^o depending on frequency. (c)Theoretical reflectivity. As opposed to model 1, before crossing, the magnitude of reflectivity decreases with increasing frequency. After crossing, the magnitude of reflectivity increases with increasing frequency; (d) The theoretical phase changes at different frequencies.

Field data example

We now show a field data example which exhibits the features seen in our modelling. The data comes from a producing gas reservoir in Vienna basin. We work with pre-stack time

migrated data which were processed to zero phase. Figure 4(a) shows a seismic image of the producing zone. Zone 1 exhibits a bright spot, corresponding to class III AVO in prestack data. The average porosity is 10% and water saturation is 78% for the reservoir interval from well log data analysis. The amplitude at Zone 2 is a little weaker than zone 1 but still brighter within the background reflections. Wells at both zones have been drilled and encountered with gas and water mixtures. Figure 4(b) showing the corresponding pre-stack common reflection point (CRP) data for zone 2. A phase reversal is clearly displayed from the seismic waveform.

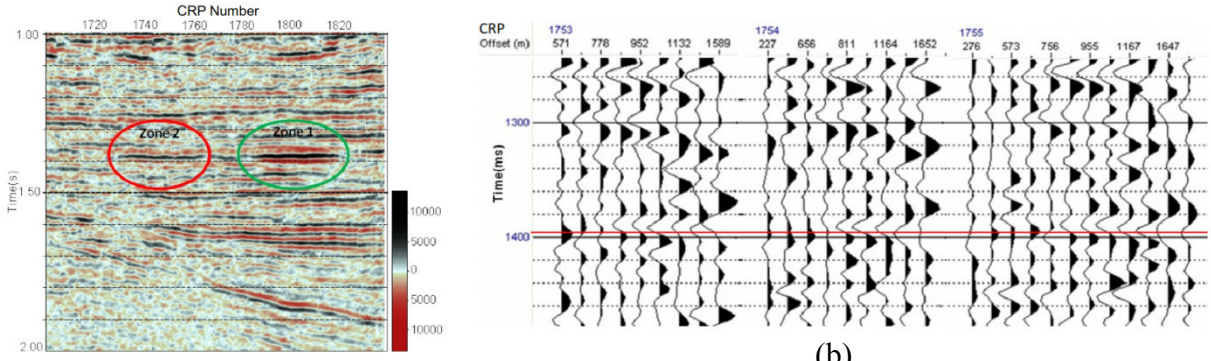

(a) (b)

Figure 4. Seismic data from a sandstone reservoir. (a) The post-stack section. Zone 1 exhibits a bright spot, corresponding to class III AVO in prestack data. The amplitude at Zone 2 is a little weaker than zone 1 but still brighter in the background reflections. Wells at both zones have been drilled and encountered gas and water mixtures. (b)Prestack time migrated CRP gathers from zone 2. The red line indicates the top of the reservoir position, which show phase reversal.

The pre-stack data were spectrally decomposed using the Wigner-Ville transform (Wu and Liu, 2009; Wu, Chapman and Li, 2014), and spectral balancing (Wilson et al. 2009) was applied to attempt to equalise the frequency content over a time window. Sufficient well log data were available to create a model for the AVO response of the reservoir. The model consisted of elastic material for the upper (shale) medium, and effective lower reservoir zone. Information on porosity, net to gross and saturation in the reservoir interval was available.

From well log data, the average porosity is 20% and water saturation is 84% for the reservoir interval. The P-wave velocity is 2.953km/s, S-wave velocity is 1.398km/s, and density is 2.40g/cm^3 for upper medium. For the lower medium, Figure 5 (a) and (b) display P-wave and S-wave velocity dispersion and attenuation. The P-wave velocity is 2.710km/s, S-wave velocity is 1.121km/s at 10Hz, and density is 2.34g/cm^3. The theoretical effective medium calculation was carried out using the equations of Chapman et al. (2002), with an effective fluid model for the saturation. Figure 5 (c) and (d) compares the theoretical curves when porosity is 20% and water saturation is 84% with the field data. The spectral amplitude (c) and phase (d) from field data are the average over nine adjacent CRP gathers around the well location in order to suppress random noise. For frequency-dependent modelling, a good qualitative match between data and model is achieved for both the frequency-dependent amplitude-versus-incident angle results and for the phase-versus incident angle results. For elastic modelling, the amplitude exhibits the feature of Class IV AVO, with a phase change from 180^o to 0^o at incident angle of 20^o. The Class IV AVO signature for Zone 2 is due to high porosity of the sandstone overlaid by hard shales.

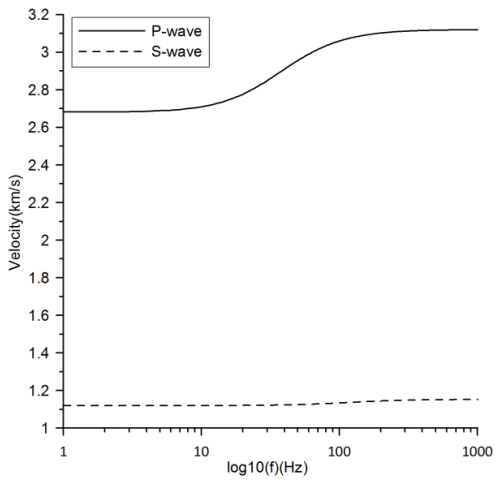

(a)

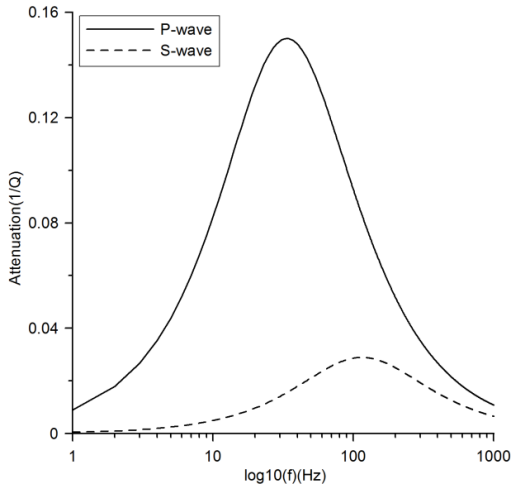

(b)

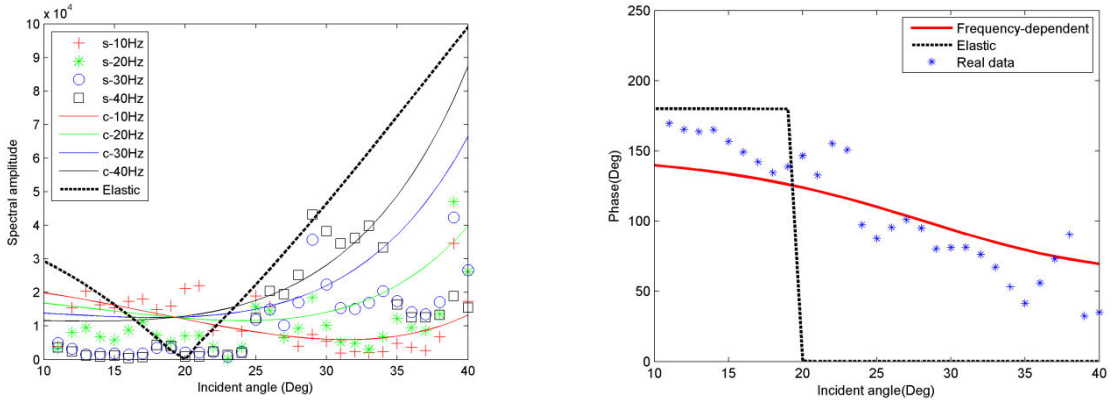

(c) (d)

Figure 5 The fitting result for the average spectral amplitude and phase from real seismic data with theoretical data and their errors distributions. (a)The P-wave and S-wave velocity dispersion for the lower medium; (b)The P-wave and S-wave attenuation (1/Q) versus frequency for the lower medium; (c) Fitting of theoretical amplitude to average spectral amplitude from seismic data at 10Hz, 20Hz, 30Hz and 40Hz. Symbols('s') are the field data, curves('c') are the theoretical reflectivity.(d) Fitting of the averaged phase derived from seismic data to the theoretical phase. A crack density of 0.14 is used for the reservoir interval to achieve the fittings. The velocities used in elastic model are vp=2.91km/s, vs=1.12km/s from frequency-dependent model when the frequency is 40Hz.

Discussion

The agreement of observation from field data with theoretical prediction suggests that fluid-induced dispersion directly and measurably influences the reflection coefficient, and that frequency-dependent rock physics models are necessary to describe the seismic properties of reservoirs containing multiple fluids. An important parameter which decides the magnitude of attenuation during fluid exchange between different pore types is the crack density ε_c. In practical analysis, the field data can be decomposed and balanced into a set of spectral amplitudes, while ε_c in our model can be used to modulate the frequency-dependence of reflectivity and calibrate to spectral amplitudes in properties-known zone, and then reservoir properties can be inverted from appraisal zone where seismic data are available. A theoretical

study of using frequency-dependent AVO for quantitative estimation of gas saturation has been presented by Wu et al. (2014). Another potential application is monitoring of CO2 saturation in brine-filled reservoir from time-lapse data. Considering velocity dispersion due to partial saturation using frequency-dependent rock physics model can be an alternative and more accurate method of estimating CO2 saturation, in addition to the standard Gassmann's theory.

Conclusions

We present a new phenomenological model for phase reversals from targets showing strong dispersion anomalies. The behaviour is markedly different from that of elastic case. Firstly, the reflection coefficient is frequency-dependent, with opposite dependence of amplitude on frequency on either side of the notional phase reversal. Secondly, the amplitude of the reflection coefficient does not touch zero around the phase reversal. Thirdly, we see a gradual continuous variation of phase with angle of incidence in place of the discontinuous change in the standard model. The field example from Vienna basin shows phase behaviour which is consistent with the frequency-dependent modelling. We believe that recognition of such phenomena from seismic data has the clear potential to improve our ability to detect fluid variations.

Acknowledgements

We would like to thank OMV Ltd for permission to show the data. We are also grateful to the two anonymous reviewers for their constructive comments. This work was supported by the sponsors of the Edinburgh Anisotropy Project (EAP), and is presented with the permission of the Executive Director of the British Geological Survey (Natural Environment Research Council).

References

Aki, K and Richards, P.G., 1980. Quantitative Seismology: W.H. Freeman and Co.

Castagna, J.P., Swan, H.W. and Foster, D.J., 1998. Framework for AVO gradient and intercept interpretation: Geophysics, 63(3), 948-956.

Chapman, M., Zatsepin, S.V. and Crampin, S., 2002. Derivation of a microstructural poroelastic model: Geophysical Journal International, 151, 427-451.

Chapman, M., Liu, E. and X.-Y., Li, 2006. The influence of fluid-sensitive dispersion and attenuation on AVO analysis: Geophysical Journal International, 167: 89-105.

Dunkin, J. W., and Levin, F. K., 1973. Effect of normal moveout on a seismic pulse: Geophysics, 38, 635-642.

Edgar, J. A. and Selvage, J. I., 2011. Can thin beds be identified using statistical phase estimation?: First break, 29, 55-65.

Innanen, K.A., 2011. Inversion of the seismic AVF/AVA signatures of highly attenuative targets: Geophysics, 76(1), R1-R14.

Kim, J., Nam, M. J. and Matsuoka, T., 2013. Estimation of CO2 saturation during both CO2 drainage and imbibition processes based on both seismic velocity and electrical resistivity measurements: Geophysical Journal International, 195, 292-300.

Korneev, V.A., Goloshubin, G.M., Daley, T.M. and Silin, D.B., 2004. Seismic low-frequency effects in monitoring fluid-saturated reservoirs, Geophysics, 69, 522–532.

Liu Y. and Schmitt D. R., (2003). Amplitude and AVO responses of a single thin bed. Amplitude and AVO responses of a single thin bed, 68, 1161-1168.

Müller, T. M., and Rothert, E., 2006. Seismic attenuation due to wave-induced flow: Why Q scales differently in random structures: Geophysical Research Letters, 33, L16305.

Müller, T. M., Gurevich, B. and Lebedev, M., 2010. Seismic wave attenuation and dispersion resulting from wave-induced flow in porous rocks–A review: Geophysics, 75(5): A147–A164.

Pride, S. R., Berryman, J. G. and Harris, J. M., 2004. Seismic attenuation due to wave-induced flow, J. Geophys. Res., 109, B01201, doi:10.1029/2003JB002639.

Quintal, B. and Tisato, N., 2013. Modeling Seismic Attenuation Due to Wave-Induced Fluid Flow in the Mesoscopic Scale to Interpret Laboratory Measurements. Fifth Biot Conference on Poromechanics, Vienna, pp. 31-40.

Quintal, B., Schmalholz, S. M., and Podladchikov, Y. Y., 2011. Impact of fluid saturation on the reflection coefficient of a poroelastic layer: Geophysics, 76(2), N1–N12

Roden R., Castagna, J. and Jones, G., 2005. The impact of prestack data phase on the AVO interpretation workflow- a case study: The Leading Edge, 24(9), 890-895.

Ross C.P. and Kinman, D.L., 1995. Nonbright-spot AVO: Two examples: Geophysics, 60, no.5, 1398-1408.

Rutherford, S.R. and Williams, R.H., 1989. Amplitude-versus-offset variations in gas sands: Geophysics, 54, 680-688.

Schoenberg, M. and Protazio, J., 1992. 'Zoeppritz' rationalized and generalized to anisotropy: Journal of Seismic Exploration, 1, 125-144.

Shuey, R.T., 1985. A simplification of the Zoeppritz equations: Geophysics, 50, 609-614.

Smith, G.C. and Gidlow, P.M., 1987. Weighted stacking for rock property estimation and detection of gas: Geophysical Prospecting, 35, 993-1014.

Taner, M. T., Koehler, F., & Sheriff, R. E., 1979. Complex seismic trace analysis: Geophysics, 44, no.6, 1041-1063.

Tisato, N and Quintal, B., 2013. Measurements of seismic attenuation and transient fluid pressure in partially saturated Berea sandstone: Evidence of fluid flow on the mesoscopic scale, Geophysical Journal International, 195(1), 342-351.

Van der Baan, M. and Fomel, S., 2009. Nonstationary phase estimation using regularized local kurtosis maximization: Geophysics, 74(6), A75-A80.

Widess, M.B., 1973. How thin is a thin bed?: Geophysics, 38(6), 1176-1180.

Wilson, A., Chapman, M. and Li, X-Y., 2009. Frequency-dependent AVO inversion: 79th annual SEG meeting Expanded Abstracts, 341-345.

Wood, A.W., 1955. A textbook of Sound. New York: Mcmillan Co.

Wu, X. and Liu, T., 2009. Spectral decomposition of seismic data with reassigned smoothed pseudo Wigner-Ville distribution, Journal of Applied Geophysics, 68(3), 386-393.

Wu X., Chapman M. and Li, X.-Y., 2014. Estimating seismic dispersion from prestack data using frequency-dependent AVO analysis. Journal of Seismic Exploration, 23 (3), 219-239.

Wu X., Chapman, M., Li X.-Y. and Boston, P., 2014. Quantitative gas saturation estimation by frequency-dependent Amplitude-Versus-Offset analysis, Geophysical Prospecting, 62 (6). 1224-1237.